Conformational Analysis of Lipophilic Antifolates: Crystal Structure of Piritrexim and a Theoretical Evaluation of Its Binding to Dihydrofolate Reductase

Paul A. Sutton and Vivian Cody*

Contribution from the Medical Foundation of Buffalo, 73 High Street, Buffalo, New York 14203. *Received February 26, 1988*

Abstract: The crystal structure of piritrexim (2,4-diamino-6-(2,5-dimethoxybenzyl)-5-methylpyrido[2,3-*d*]pyrimidine; PTX), an effective antineoplastic lipophilic antifolate, was determined to examine its conformational features and its mode of binding to the enzyme dihydrofolate reductase (DHFR). The molecular conformation of PTX shows that the orientation of the dimethoxybenzyl and pyridopyrimidine rings are twist ($\tau_1/\tau_2 = -76.3/146.0°$) about the methylene bridge. The pyridopyrimidine rings form antiparallel stacking arrangements in the lattice and form a network of N···N hydrogen bonds. A theoretical study of the molecular characteristics of PTX binding to chicken liver DHFR was carried out by using the program YETI to optimize DHFR–PTX interactions. These studies indicate that there are two slightly different perpendicular (e.g., $\tau_1/\tau_2 \simeq -131/-105°$ and $-98/-105°$) conformers of PTX which have two modes of binding, independent of the orientation of Tyr-31. While these binding studies show a perference for a perpendicular PTX conformation (i.e., $\tau_1/\tau_2 \simeq 90/90°$), which differs from that observed in the crystal structure, there is less than 2.5 kcal/mol energy difference between them.

Piritrexim (PTX; 2,4-diamino-6-(2,5-dimethoxybenzyl)-5-methylpyrido[2,3-*d*]pyrimidine), first reported by Grivsky et al.,[1] is now in phase II clinical studies as a lipid-soluble substitute for the antineoplastic drug methotrexate (MTX).[2] Unlike, MTX, PTX is not dependent upon uptake systems to enter cancer cells. This ability to bypass the folate transport mechanism is important because tumor cells are able to develop resistance to MTX by virtue of an impaired transport mechanism. Additionally, tumor cells can become resistant to MTX via alterations in the target enzyme; fortunately this form of resistance can be overcome by using lipophilic antifolates.[3] However, many lipophilic antifolates show side effects not associated with MTX. This additional toxicity of lipophilic antifolates has been traced to their ability to inhibit histamine *N*-methyltransferase, causing side effects including severe headache, skin rash, and gastric discomfort.[4] The search for a lipophilic antifolate with poor affinity for histamine *N*-methyltransferase, while maintaining activity comparable to that of MTX, led to the discovery of PTX. More recently PTX has found promise in the treatment of *T. gondii*[5] and *P. carnii*,[6] the former of which is an opportunistic infection in patients with AIDS.

Antifolates act by inhibiting dihydrofolate reductase (DHFR), an enzyme necessary for all cell growth.[7] As such, antifolates are important in cancer chemotherapy and in the treatment of microbial infections. Because of the therapeutic advantages of designing antifolates with specific affinity for different species of DHFR enzymes, the three-dimensional structure of DHFR has been determined from bacterial,[8,9] avian,[10] and mammalian[11] sources. These structural data provide the basis to better understand substrate–receptor interactions and thus facilitate the design of more efficient drugs.

Several groups have been successful in predicting structural modifications of antifolates on the basis of protein structural data. With the aid of computer graphics and molecular modeling, Kyper et al.[12] were able to target a specific protein–substrate interaction by selectively modifying the antibacterial trimethoprim (TMP). Although computer graphics visualization can provide a qualitative basis to predict structural modification likely to improve binding affinity, theoretical approaches which incorporate physical and chemical properties of protein–ligand interactions offer a higher level of accuracy in inhibitor design. This is particularly important when both the substrate and receptor have conformational flexibility,[13] and similar ligands have the ability to bind to the receptor in different orientations.[14] A variety of theoretical approaches for the study of substrate–receptor interactions have been developed and several of these methods have been applied to studies involving antifolate–DHFR interactions.[15]

The goal of this study is to determine the structural properties of DHFR antagonists so as to gain a better understanding of their biological properties. Therefore, we report the single-crystal structure of PTX, as well as its theoretically modeled binding interactions with chicken liver DHFR. We have utilized the program YETI,[16] which incorporates a hydrogen-bonding function into its energy term which is based on hydrogen-bond characteristics of small-molecule molecular packing,[16c] to study PTX–DHFR interactions.

*Send reprint requests to: Dr. Vivian Cody, Medical Foundation of Buffalo, 73 High St., Buffalo, NY 14203.

(1) Grivsky, E. M.; Lee, S.; Sigel, C. W.; Duch, D. S.; Nichol, C. A. *J. Med. Chem.* **1980**, *23*, 327.
(2) Duch, D. S.; Edelstein, M. P.; Bowers, S. W.; Nichol, C. A. *Cancer Res.* **1982**, *42*, 3987.
(3) Hamrell, M. R. *Oncology*, **1984**, *41*, 343.
(4) Duch, D. S.; Edelstein, M. P.; Nichol, C. A. *Mol. Pharmacol.* **1980**, *18*, 100.
(5) Araujo, F. G.; Guptill, D. R.; Remington, J. S. *J. Infect. Dis.* **1987**, *156*, 828.
(6) Queener, S. F.; Bartlett, M. S.; Jay, M. A.; Durkin, M. M.; Smith, J. W. *Antimicrob. Agents Chemother.* **1987**, *31*, 1323.
(7) For a review, see: (a) Blakley, R. L.; Benkovic, S. J. *Folates and Pterins*; Wiley: New York, 1984; Vol. 1. (b) Blaney, J. M.; Hansch, C.; Silipo, C.; Vittoria, A. *Chem. Rev.* **1984**, *84*, 333 and references therein.
(8) Bolin, J. T.; Filman, D. J.; Matthews, D. A.; Hamlin, R. C.; Kraut, J. *J. Biol. Chem.*, **1982**, *257*, 13650.
(9) Matthews, D. A.; Bolin, J. T.; Burridge, J. M.; Filman, D. J.; Volz, K. W.; Kaufman, B. T.; Beddell, C. R.; Champness, J. N.; Stammers, D. K.; Kraut, J. *J. Biol. Chem.* **1985**, *260*, 381.
(10) (a) Voltz, K. W.; Matthews, D. A.; Alden, R. A.; Freer, S. T.; Hansch, C.; Kaufman, B. T.; Kraut, J. *J. Biol. Chem.* **1982**, *257*, 2528. (b) Matthews, D. A.; Bolin, J. T.; Burridge, J. M.; Filman, D. J.; Volz, K. W.; Kraut, J. *J. Biol. Chem.* **1985**, *260*, 392.
(11) Stammers, D. K.; Champness, J. N.; Beddell, C. R.; Dann, J. G.; Eliopoulos, E.; Geddes, A. J.; Ogg, D.; North, A. C. T. *FEBS Lett.* **1987**, *218*, 176.
(12) Kyper, L. F.; Roth, B.; Baccanari, D. P.; Ferone, R.; Beddell, C. R.; Champness, J. N.; Stammers, D. K.; Dann, J. G.; Norrington, F. E.; Baker, D. J.; Goodford, P. J. *J. Med. Chem.* **1985**, *28*, 303.
(13) McCammon, J. a. *Rep. Prog. Phys.* **1984**, *47*, 1.
(14) Selassie, C. D.; Fang, Z-X.; Li, R-L.; Hansch, C.; Klein, T.; Langridge, R.; Kaufman, B. T. *J. Med. Chem.* **1986**, *29*, 621.
(15) (a) DesJarlais, R. L.; Sheridan, R. P.; Dixon, J. S.; Kuntz, I. D.; Venkataraghavan, R. *J. Med. Chem.* **1986**, *29*, 2149. (b) Goodford, P. J. *J. Med. Chem.* **1985**, *28*, 849.
(16) (a) Vedani, A. *J. Comput. Chem.* **1988**, *9*, 269. (b) Vedani, A.; Dobler, M.; Dunitz, J. D. *J. Comput. Chem.* **1986**, *7*, 701. (c) Vedani, A.; Dunitz, J. D. *J. Am. Chem. Soc.* **1985**, *107*, 7653.

0002-7863/88/1510-6219$01.50/0

Experimental Section

X-ray Structure Determination. PTX (BW301) was a gift from Burroughs-Wellcome & Co. Crystals of PTX were grown from ethanol with trace amounts of ethanolamine. The crystal data show the following: space group *Pbca*, orthorhombic, $a = 13.389$ (2) Å, $b = 25.021$ (4) Å, $c = 9.566$ (2) Å, $V = 3184.72$ Å^3, $Z = 8$, $D_{calcd} = 1.357$ g cm^{-1}. The crystal used for data collection was rectangular with dimensions 0.24 × 0.60 × 0.90 mm. Data were collected on a Nicolet P3 diffractometer using Mo Kα radiation. The crystal was stable and showed no deterioration during data collection. The X-ray diffraction data were corrected for Lorentz and polarization effects but not for extinction or absorption effects. A total of 3681 unique reflections were collected to $2\theta = 130°$. The structure was solved by using the direct methods programs MULTAN[17] and NQEST.[18] Non-hydrogen atom thermal parameters were made anisotropic and refined by full-matrix least-squares techniques. Hydrogen atoms were located in Fourier difference maps and were given isotropic thermal parameters one unit greater than the heavy atoms to which they were bound; their thermal parameters were held constant during refinement. The final R value was 0.054 for 2248 data with $I > 3\sigma(I)$.

Molecular Modeling. Modeling studies with chicken liver DHFR[10,19] were performed on an active-site region comprising the following residues: 6–10, 16–22, 24–35, 38, 50–53, 55–68, 113–117, 121, 134–136, 138, 172, 177, 179, and NADPH. Structural waters (between 2.3 and 3.2 Å from the amino acid residues or the substrate) were included in the evaluation. Waters that fit this requirement were 233, 335, 424, and 629. The active-site region was selected by the program PICK[16a] to lie within 7 Å of the substrate molecule. The location of the substrate molecule was estimated by docking PTX into the active site of the protein by using molecular modeling techniques.[20]

Molecular Mechanics. Substrate–protein interactions were evaluated on the basis of electrostatic, van der Waals, and H-bonding interactions by using the program YETI (version 2.5).[16] YETI allows translational and rotational freedom of the substrate and water and allows conformational freedom of the amino acid side chains and substrate. Since the program is not designed to vary the protein's main chain, conformational freedom of the protein was restricted to residues within 4 Å of the ligand. Those amino acid side chain allowed conformational freedom were 7, 8, 21, 22, 30, 31, 34, 64, and 67. Water refinement (233, 335, 424, and 629) proceeded by first allowing rotational freedom to optimize donor–acceptor interactions. Once donor–acceptor directionality was found, we allowed translational freedom to optimize the distance criteria. For NADPH, only the amide was allowed conformational freedom while no translational freedom was given.[21]

Vedani and Dunitz[16c] incorporated the hydrogen-bonding function into the energy term of YETI to avoid problems associated with assigning atomic partial charges and artificial dielectric constants. By ignoring the electrostatic contribution, the energy term relies on parameters derived from structural data, such as nonbonded distances, coordination geometries at metal centers, and hydrogen-bond geometries. Since binding of antifolates to DHFR involves an ionic interaction, the electrostatic contribution was included in these calculations. YETI assigns standard partial charges to the amino acids and waters. Partial charges of PTX were determined with the Gaussian 80 system of programs and the STO-3G basis set.[22] The contribution of the electrostatic potential to the energy term was controlled by using 4 for the dielectric constant. A range (2–6) of values for the dielectric constants was investigated such that the distance of the ionic interaction between PTX and DHFR approached values seen in small molecule intermolecular hydrogen bond data.

Potential energy calculations for the rotation about C(5)–C(9) and C(9)–C(10) bonds were done with CHEMMODEL.[21] The potential energies were calculated over the full 360° range at steps of 10° for each bond, while the geometry was held fixed as observed in the crystal structure.

Table I. Atomic Coordinates (Non-Hydrogen, ×10^4; Hydrogen, ×10^3) and Isotropic Thermal Parameters (Å^2 × 10^2) for Piritrexim

atom	x/a	y/b	z/c	B_{eq}[a]
C(2)	4061 (1)	241 (1)	13147 (2)	329 (5)
C(4)	5483 (1)	554 (1)	12092 (2)	328 (5)
C(4A)	4945 (1)	636 (1)	10788 (2)	281 (5)
C(5)	5313 (1)	859 (1)	9518 (2)	338 (5)
C(6)	4687 (2)	877 (1)	8369 (2)	382 (6)
C(7)	3721 (2)	679 (1)	8532 (2)	429 (6)
C(8A)	3935 (1)	464 (1)	10841 (2)	306 (5)
C(9)	4994 (2)	1098 (1)	6958 (2)	488 (7)
C(10)	5026 (2)	1704 (1)	6894 (2)	406 (6)
C(11)	5734 (2)	1962 (1)	6064 (2)	460 (7)
C(12)	5746 (2)	2508 (1)	5981 (3)	574 (8)
C(13)	5063 (2)	2811 (1)	6731 (3)	537 (8)
C(14)	4371 (2)	2565 (1)	7564 (2)	458 (7)
C(15)	4354 (2)	2013 (1)	7630 (2)	447 (6)
C(51)	6356 (2)	1074 (1)	9364 (3)	498 (7)
C(111)	7120 (2)	1867 (1)	4495 (3)	681 (9)
C(141)	3784 (2)	3377 (1)	8571 (3)	623 (8)
N(1)	3489 (1)	269 (1)	12015 (2)	315 (4)
N(2)	3646 (1)	81 (1)	14382 (2)	427 (5)
N(3)	5046 (1)	365 (1)	13234 (2)	348 (5)
N(4)	6465 (1)	666 (1)	12221 (2)	493 (6)
N(8)	3330 (1)	483 (1)	9701 (2)	395 (5)
O(11)	6385 (1)	1632 (1)	5361 (2)	696 (6)
O(14)	3663 (1)	2823 (1)	8363 (2)	651 (6)
H(N2A)	403 (2)	−5 (1)	1513 (2)	
H(N2B)	302 (2)	−10 (1)	1440 (2)	
H(N4A)	673 (2)	57 (1)	1303 (2)	
H(N4B)	678 (2)	72 (1)	1138 (2)	
H(7)	326 (2)	68 (1)	773 (2)	
H(9A)	450 (2)	97 (1)	630 (2)	
H(9B)	571 (2)	96 (1)	671 (2)	
H(12)	628 (2)	269 (1)	541 (2)	
H(13)	510 (2)	318 (1)	667 (3)	
H(15)	387 (2)	185 (1)	822 (2)	
H(51A)	683 (2)	79 (1)	925 (3)	
H(51B)	643 (2)	129 (1)	851 (3)	
H(51C)	656 (2)	129 (1)	1012 (2)	
H(111A)	755 (2)	214 (1)	499 (3)	
H(111B)	753 (2)	156 (1)	419 (3)	
H(111C)	676 (2)	209 (1)	377 (3)	
H(141A)	366 (2)	359 (1)	761 (3)	
H(141B)	330 (2)	346 (1)	933 (3)	
H(141C)	450 (2)	347 (1)	884 (3)	

[a] $B_{eq} = {}^4/_3\sum_i\sum_j\beta_{ij}(a_i a_j)$.

Results

Heavy atom positions of PTX are listed in Table I. Its molecular conformation (Figure 1) is twist and is described by the torsion angles τ_1[C(5)–C(6)–C(9)–C(10) = −76.3°] and τ_2[C(6)–C(9)–C(10)–C(11) = 146.0°], which places the benzyl group nearly perpendicular (100°) to the pyridopyrimidine ring. A similar conformation is seen in the only other structurally similar pyridopyrimidine (2,4-diamino-5-methyl-6-benzylpyrido[2,3-*d*]-pyrimidine; BPP),[23] for which $\tau_1/\tau_2 = -88.8/144.8°$; in addition, PTX has a conformation similar to that of several antibacterial trimethoprim (2,4-diamino-5-(3,4,5-trimethoxybenzyl)pyrimidine) structures.[24] The 10 atoms of the pyridopyrimidine ring are planar (rms = 0.003 Å), while the N(2), N(4), C(51), and C(9) deviate

(17) Germain, G.; Main, P.; Woolfson, M. M. *Acta Crystallogr., Sect. A* **1971**, *A27*, 368.

(18) De Titta, G. T.; Edmonds, J. W.; Langs, D. A.; Hauptman, H. A. *Acta Crystallogr., Sect. A* **1975**, *A31*, 472.

(19) Coordinates of chicken liver DHFR holoenzyme were supplied by Oatley, S. J.; Matthews, D. A.; Burridge, J. M. (private communication). These coordinates are from X-ray data refined to 1.7-Å resolution and include NADPH and water.

(20) Solvent accessible surfaces were computed by using procedures developed by M. Connolly (*Science (Washington, D.C.)* **1983**, *221*, 709) and displayed on the MMS-X graphics display system, designed and fabricated by the Computer Systems Laboratory, Washington University, St. Louis. This system was made possible by a grant (RR-00396) from the Division of Research Resources, NIH, under their Biotechnology Resources Program.

(21) This version of YETI recognizes only amino acid residues, water, and a metal; the substrate is defined by the user. As such, NADPH is not recognized by YETI and thus could not be incorporated during refinement of PTX–DHFR interactions. Since NADPH does contribute to the active-site surface, we included that part of the coenzyme in contact with the ligand to be a glutamine and the γ-amine was allowed rotational freedom.

(22) Chem-X, developed and distributed by Chemical Design Ltd, Oxford, England. Gaussian 80 through Chem-X (Chandra Sing, U.; Kollman, P. *QCPE Bull.* **1982**, *2*, 117). Because of space restrictions on the computer system, PTX was divided into two structural fragments—2,4-diamino-5,6-dimethylpyrido[2,3-*d*]pyrimidine and 2,5-dimethoxytoluene—for the determination of partial charges. The geometry of the structure was held constant during the calculation of the partial charges; therefore, the charges are not likely to vary from values obtained by using the entire structure in the calculations. Since antifolates are known to be protonated while bound to the active site of DHFR, we determined partial charges for the N(1) protonated pyridopyrimidine.[7]

(23) Cody, V. *Acta Crystallogr., Sect. C* **1984**, *C40*, 1000.

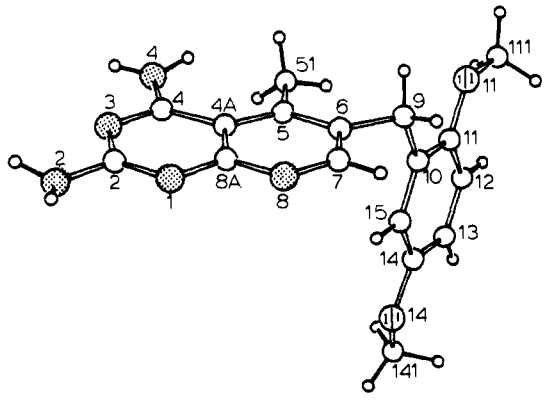

Figure 1. Atomic numbering and molecular conformation of PTX. The stippled circles are N and the dashed circles O.

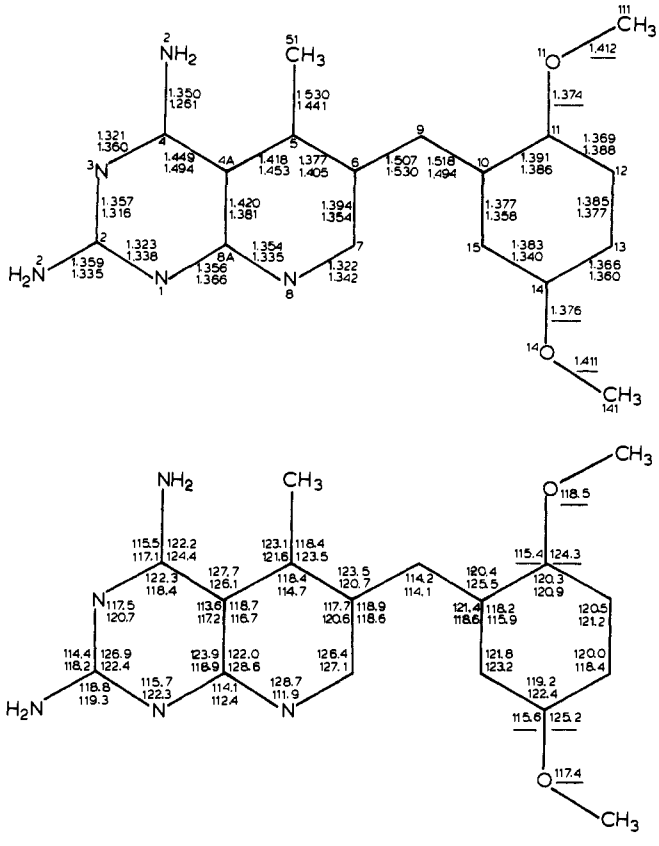

Figure 2. Bond distances and angles for PTX (top) and BPP (bottom). The average esd's for PTX bond lengths and angles are ±0.003 and ±0.2, respectively.

from this plane by only 0.15, −0.12, 0.11, and 0.05 Å, respectively. Atoms of the 11,14-dimethoxybenzyl ring deviate by less than 0.013 Å from the plane (defined by atoms C(10) through C(15)); two exceptions are O(141) and C(9), which deviate from the ring plane by about 0.3 Å.

Generally, bond lengths and angles of pyrimidine,[25,26] pteridine,[27] and quinazoline[28] antifolates reflect their protonation state. The differences between protonated and nonprotonated antifolates

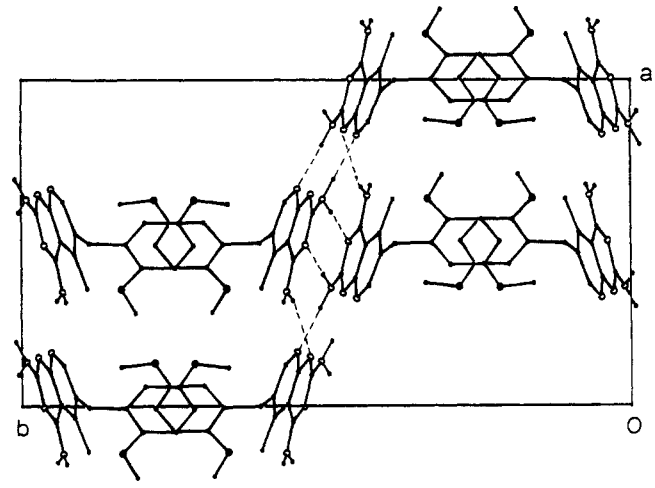

Figure 3. Molecular packing and hydrogen bonding interactions of PTX (larger open circules are nitrogen and larger closed circles are oxygens) and pyridopyrimidine ring stacking.

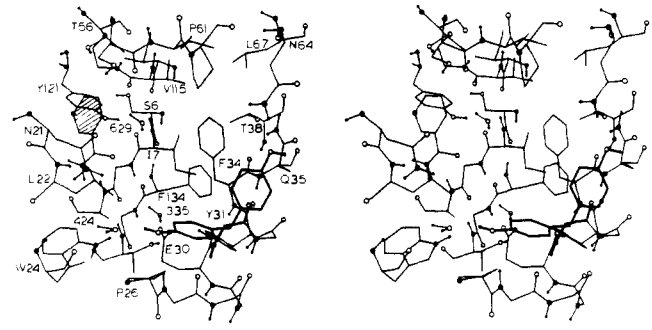

Figure 4. Active site region (6 Å) of chicken liver DHFR. The heavy lines show both orientations of Tyr-31, and the shaded structure is the nicotinamide portion of NADPH.

are manifested by shortening of the exocyclic amino bonds and lengthening of the adjacent endocyclic C–N bonds, in addition to large angular changes at the N(1), C(2), and C(8A) positions. A similar pattern is seen in the geometry of the PTX free base and the N(1) protonated salt of BPP (Figure 2). Other significant differences include the C(7)–N(8)–C(8A) angle and C(4)–N(4) bond length.

The molecular packing of PTX is depicted in Figure 3. The pyridopyrimidine rings are stacked in an antiparallel arrangement which places the ring planes at a distance of 3.38 Å; a nearly identical ring stacking is seen in the antifolate trimetrexate.[28] The N(2) nitrogen donates two hydrogen bonds [N(2)···N(3), 3.073 Å and N(2)···N(8), 3.013 Å] and interactions with N(3) set up a pseudo-base-pair hydrogen-bonding pattern which has been observed in several pyrimidine antifolate structures.[24,25] The N(4) nitrogen forms only one hydrogen-bonding interaction [N(4)···N(1), 2.976 Å] since a second hydrogen bond is prevented by the steric interactions of the C(5) substituent and is similarly observed in the 5-methylquinazoline antifolate trimetrexate.[28]

Molecular Refinement

Figure 4 shows the active-site cleft of chicken liver DHFR.[10] The opening has three hydrophilic residues—Asn-21, Asn-64, and, to a lesser extent, Tyr-31. Three hydrophobic residues (Pro-25, -26, and -61) also line the surface of the active site. Crystal structure results of DHFR–inhibitor complexes reveal that the orientation of Tyr-31 is dependent upon the structure of the inhibitor.[9-11] The vertebrate DHFR crystal structures, including the holoenzyme used in this study, have Tyr-31 (Phe-31 in mammals) in a position which is parallel to Phe-34.[9-11] With trimethoprim bound to the active site of chicken liver DHFR, Tyr-31 is perpendicular to Phe-34[9,10] (Figure 4). Tyrosine-31 in

(24) Sternglanz, H.; Bugg, C. E. *Acta Crystallogr., Sect. B* **1973**, *B29*, 2191.
(25) Schwalbe, C. H.; Cody, V. In *Chemistry and Biology of Pteridines*; Blair, J. A. Ed.; Walter de Gruyter: New York, 1983, pp 511–515.
(26) Cody, V.; Sutton, P. A.; Welsh, W. J. *J. Am. Chem. Soc.* **1987**, *109*, 4053.
(27) Cody, V.; Sutton, P. A.; Smith, G. D. *J. Am. Chem. Soc.* **1986**, *108*, 4155.
(28) Sutton, P. A.; Cody, V. *J. Med. Chem.* **1987**, *30*, 1843.

Table II. PTX Conformation (deg) When Refined in the Chicken Liver DHFR Active Site

torsion angle	refinement conditions[a] A	B	C	D	PTX[b]
τ_1[C5-C6-C9-C10]	-132.1	-97.8	-129.9	-99.4	-76.3
τ_2[C6-C9-C10-C11]	-107.0	-103.7	-101.5	-104.6	146.0
τ_3[C10-C11-O11-C111]	-166.3	-151.3	-167.9	-151.1	179.7
τ_4[C13-C14-O14-C14]	-17.2	26.4	-11.2	27.4	-13.8

[a] A: Tyr-31 parallel to Phe-34, no water-629. B: Tyr-31 parallel to Phe-34, water-629 included. C: Tyr-31 perpendicular to Phe-34, no water-629. D: Tyr-31 perpendicular to Phe-34, water-629 included. [b] Crystal structure torsion angles.

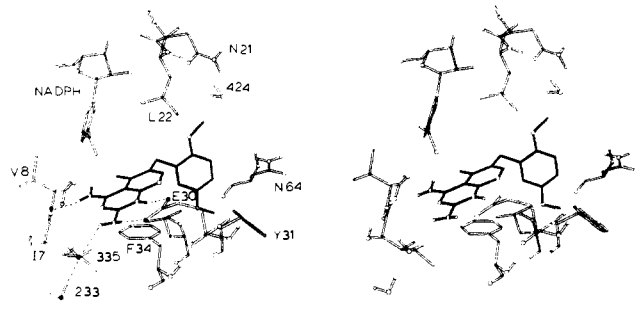

Figure 5. Orientation and conformation of PTX in the active site of DHFR with Tyr-31 parallel to Phe-34 and without water-629. Residues within 4 Å of PTX are included and those oxygens of the protein hydrogen bonded to PTX are filled in. (See refinement A in Table III for polar interactions.)

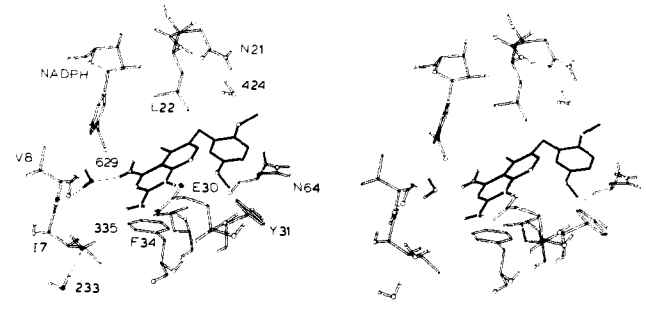

Figure 6. Orientation and conformation of PTX in the active site of DHFR with Tyr-31 parallel to Phe-34 and water-629 is included. Residues within 4 Å of PTX are included and those oxygens of the protein hydrogen bonded to PTX are filled in. (See refinement B in Table III for polar interactions.)

the perpendicular position places the phenol ring over Pro-26 and uncovers Gln-35. The floor of the active site is largely hydrophilic and includes Glu-30, Trp-24, Thr-136, water-335, and water-424. Glutamate-30 participates in an ionic interaction with antifolates. Other important hydrophilic interactions between the protein and inhibitor are through main-chain oxygens and nitrogens (i.e., Val-8, Ala-9, and Val-115) and the coenzyme. In contrast, the remaining residues in contact with the inhibitor (Phe-34, Leu-22, Ile-7, and Val-115) are hydrophobic.

Water-629 is hydrogen bonded to the carbonyl oxygens of Ile-7 and Val-115 in the holoenzyme and was included in part of the modeling studies to limit the depth of ligand penetration while maintaining a hydrogen-bonding bridge between the protein and inhibitor. Crystal structure data, however, show water-629 to be displaced from the active site when the antifolate is bound.[10]

PTX–DHFR interactions were investigated with respect to both orientations of Tyr-31 and inclusion/exclusion of water-629. Refinement of PTX in the active site of DHFR with either Tyr-31 orientation had only a minor effect on the final conformation and orientation of PTX, as the average atomic shift of PTX was less than 0.5 Å between energy-minimization conditions (Table II, compare A with C and B with D). The results of these four refinement conditions are shown in Figures 5–8. When water-629 is included, there is a significant loss in protein–substrate interactions; however, these losses are nearly compensated for by interactions created by the water and the new PTX position.

Without water-629, PTX refines to a position about 2 Å deeper in the active-site clef. The conformation and orientation of PTX and many DHFR–PTX interactions differ with the depth of penetration (Tables II and III). The set of protein–PTX interactions maintained regardless of refinement conditions are two O···N interactions between the γ-carboxylic acid of Glu-30 and the N(1) and N(2) positions of PTX (Figures 4–8). The distances of this two-point interaction are consistent throughout the four refinements and are similar to those of TMP bound to the active site of DHFR (Table III). The final distances of this ionic interaction were sensitive to the value of the dielectric constant; thus several values (2–6) were tested to select one that resulted in contact distances approaching those observed for small molecules. The average distances in small molecule crystal structures having

Table III. Polar Interaction (Å) of PTX and Trimethoprim (TMP) in the Chicken Liver DHFR Active Site[19]

residue	protein–ligand interaction	refinement conditions[a] A	B	C	D	TMP
Glu-30	OE2···N(1)	2.89	2.86	2.87	2.92	2.8
Glu-30	OE1···N(2)	2.88	2.86	2.89	2.84	2.5
water-335	O···N(2)	2.90	4.94	2.85	5.67	
Val-8	N···N(3)	3.45		3.47		3.0
Ile-7	O···N(4)	2.76		2.79		3.0
NADPH	O···N(4)	2.99	3.90	3.01	3.83	2.7
Wat-629	O···N(4)		2.73		2.74	
Gln-35	NH···O(114)	3.64		3.64		
Asn-21	NH···O(111)		3.74		3.38	
Asn-64	NH···O(114)		3.57		3.60	

[a] A: Tyr-31 parallel to Phe-34, no water-629. B: Tyr-31 parallel to Phe-34, water-629 included. C: Tyr-31 perpendicular to Phe-34, no water-629. D: Tyr-31 perpendicular to Phe-34, water-629 included.

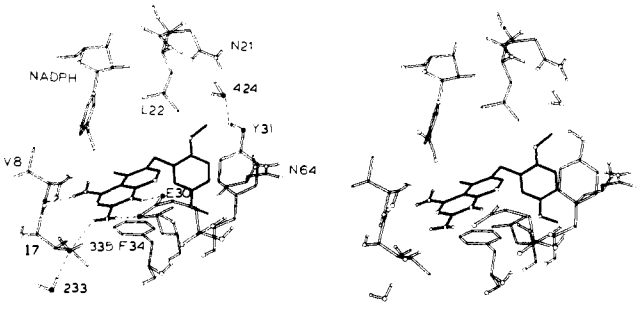

Figure 7. Orientation and conformation of PTX in the active site of DHFR with Tyr-31 perpendicular to Phe-34 and no water-629. Residues within 4 Å of PTX are included and those oxygens of the protein hydrogen bonded to PTX are filled in. Note that Tyr-31 is hydrogen bonded to water-424. (See refinement C in Table II for polar interactions.)

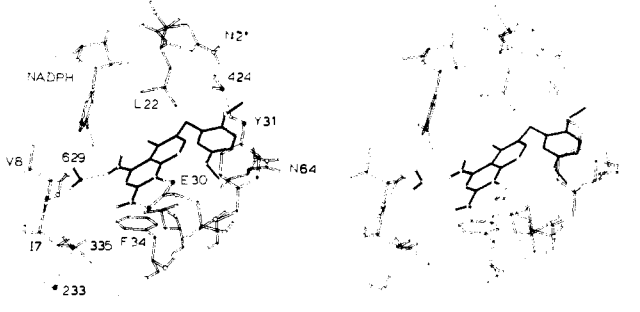

Figure 8. Orientation and conformation of PTX in the active site of DHFR with Tyr-31 perpendicular to Phe-34 and water-629 is included. Residues within 4 Å of PTX are included and those oxygens of the protein hydrogen bonded to PTX are filled in. Note that Tyr-31 is hydrogen bonded to water-424. (See refinement D in Table III for polar interactions.)

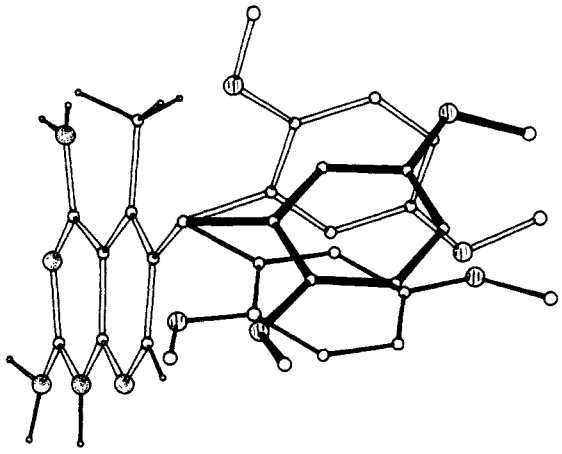

Figure 9. Conformational comparison of PTX: open lines from crystal structure, heavy lines from refinement conditions A and C, and narrow lines from refinement conditions B and D.

this two-point carboxylic acid–antifolate ionic interaction are 2.66 and 2.80 Å for N(1)···O and N(2)···O, respectively.[29] The N(1)···O and N(2)···O distances for TMP bound to chicken liver DHFR are 2.8 and 2.5 Å, respectively (Table III), which are reversed from the small molecule data.

This two-point [N(1)···O and N(2)···O] interaction plays a significant role in antifolate binding affinity. Loss of this interaction has been studied by site-specific mutagenesis in which an acid residue (Arg-27) of *Escherichia coli* DHFR is replaced by an alcohol residue (Ser-27).[30] The decrease in binding energy of methotrexate was shown to be 4.4 kcal/mol.

In refinements A and C (Table III), several interactions are similar to those found in bacterial and mouse DHFR crystal structures.[8-11] In addition to the interactions noted above, N(2) hydrogen bonds to a structural water in both bacterial and mouse DHFR. The carbonyl of an isoleucine residue hydrogen bonds to the N(4) position of the antifolate in all DHFR crystal structures. Although the N(4) position of PTX is within hydrogen-bonding distance to the carbonyl oxygen of the amide portion of NADPH, this interaction does not make any significant contribution to the binding of the ligand because of the poor hydrogen bonding directionality (O···H-N(4) = 83°). In mouse DHFR,[11] the N(4) position of MTX makes a hydrogen-bonding contact with Val-115, an interaction also seen in bacterial DHFR[8-10] but not seen in these modeling studies. In C(5)-substituted quinazoline and pyridopyrimidine antifolate crystal structures (as in PTX), N(4) accepts only one hydrogn bond;[24,28] therefore, the single hydrogen bond to N(4) observed in this study is consistent with small molecule packing characteristics. Trimethoprim also accepts only one hydrogen bond when bound to the chicken liver enzyme, and this is considered an important factor in its decreased binding affinity for the enzyme.[9]

Without water-629 in the active site, the dimethoxybenzyl ring of PTX is in a hydrophobic environment and is in agreement with modeling studies of PTX–chicken liver DHFR made by Blaney et al.[7b] A potential polar interaction between Gln-35 with PTX (Table III) is blocked when Tyr-31 is parallel to Phe-34 (Figure 4). Even though the perpendicular position of Tyr-31 uncovers Glu-35, this residue is strongly hydrogen bonded to Arg-70, and as such, there is very little conformational freedom to optimize interactions with PTX. With water-629 included, PTX moves into a position where both methoxy groups make polar contacts with γ-amides of two asparagine residues (Asn-21 and Asn-64, Table III, and Figures 6 and 8). In addition to the polar contact

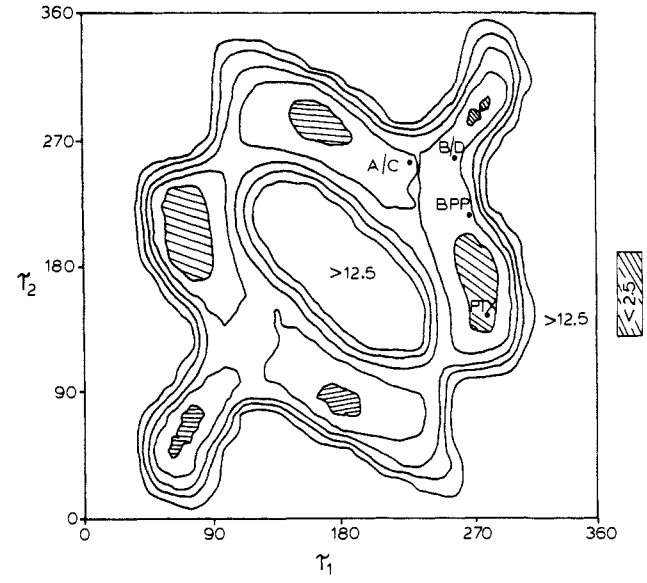

Figure 10. Two-dimensional energy map of PTX showing the location of the various conformers with respect to rotational barriers. Each line represents an increase of 2.5 kcal/mol from the relative energy minimum.

with Asn-21, O(11) of refinement D has an additional polar contact with the phenol oxygen of Tyr-31 (4.2 Å, Figure 8). Although methoxy groups act as hydrogen-bond acceptors in small molecule crystal structures,[28] the proper orientation of PTX with respect to hydrophilic residues was not found in this study because the methyl groups tended to prevent optimum hydrogen bonding interactions.

Visually docking PTX into the active site of DHFR without water-629 yielded a conformer which was very similar to conformers A and C (Table II). Conformational energy minimization of PTX in the active site of DHFR was carried out with this docked structure. The orientation of Tyr-31 caused only minor conformational adjustments of PTX (Table II, compare A with C and B with D), whereas the depth of PTX penetration resulted in major conformational differences (Table II, compare A with B and C with D), particularly with τ_1 and the C(14) (τ_4) methoxy group. Since there are only slight conformational differences between conformers A and C and between conformers B and D, we refer to these two sets of conformers as (A/C) and (B/D). The conformational differences of these two groups are shown in Figure 9.

A potential energy map of PTX (Figure 10) shows that the rotational barriers between conformers are relatively small. Although the crystal structure conformation is in the lowest energy level, there is less than a 2 kcal/mol difference between it and the conformational energy levels of conformers A/C and B/D. Conformers A/C and B/D differ in conformational energy by less than 1 kcal/mol (A/C < B/D).

Summary

The molecular conformation of PTX at the methylene bridge has a twist conformation which places the dimethoxybenzyl in a perpendicular orientation with respect to the pyridopyrimidine ring. The pyridopyrimidine rings form antiparallel stacking arrangements in the lattice and form a network of N···N hydrogen bonds. The crystal structure of PTX and related antifolates[24-29] allows us to define ligand–protein interactions. The YETI hydrogen-bonding functionality incorporates small molecule crystal structure data to the energy term and as a result optimum donor–acceptor interactions are defined by experimental data. This lowers the reliance on theoretical (electrostatic) contributions to the energy terms. However, atomic partial charges, along with the related dielectric parameter, were necessary to fully exploit the ionic nature of the PTX–DHFR interaction. The hydrophilic PTX–DHFR interactions determined with YETI are consistent with both ligand-bound protein structures and packing characteristics

(29) Average values for seven N···O distances from: (a) Bryant, P. K.; Colby, J.; Jenks, R. G.; Lowe, P. R.; Schwalbe, C. H. *Acta Crystallogr., Sect. A* **1984**, *A37*, S79. (b) Giuseppetti, G.; Tadini, C. *Acta Crystallogr., Sect. C* **1984**, *C40* 650. (c) Reference 27.

(30) Howell, E. E.; Villafranca, J. E.; Warren, M. S.; Oatley, S. J.; Kraut, J. *Science (Washington, D.C)* **1986**, *231*, 1123.

of antifolates in general. YETI provides an easy method to analyze the energy of ligand-protein interactions and permits quick optimization of these interactions.

In summary, our modeling studies show that Tyr-31 can exist in either orientation with respect to PTX binding. However, when Tyr-31 is perpendicular to Phe-34, its phenol oxygen contributes to a hydrophilic environment for PTX, which suggests that the perpendicular orientation may be favorable. In the perpendicular position, the phenol oxygen of Tyr-31 hydrogen bonds with water-424; however, in mammalian DHFR this potential hydrogen bond is lost because residue 31 is a phenylalanine. As such, advantages of the perpendicular position for Tyr-31 are lost for the mammalian enzymes. These studies indicate that there are two slightly different perpendicular (e.g., $\tau_1/\tau_2 \simeq -131/-105°$ and $-98/-105°$) conformers of PTX which have two modes of binding that are independent of the orientation of Tyr-31. While these binding studies show a preference for a perpendicular PTX conformation (i.e., $\tau_1/\tau_2 \simeq 90/90°$), which differs from that observed in the crystal structure, there is less than 2.5 kcal/mol energy difference between them.

Acknowledgment. This work was supported in part by grants from NCI-CA34714, and FRA-287 (VC) from the American Cancer Society Faculty Research Award.

Supplementary Material Available: Tables of anisotropic thermal parameters, hydrogen-bonding geometry, and atomic partial charges (2 pages); lists of structure factor calculations (14 pages). Ordering information is given on any current masthead page.

Kinetic Solvation Pressure: A Measure of Environmental Effects on Reaction Rates. 1. Application to Hydrophobic Systems[1,2]

Julio F. Mata-Segreda[2]

Contribution from the School of Chemistry, University of Costa Rica, San Pedro 2060, Costa Rica. *Received October 23, 1984*

Abstract: A quantity termed kinetic solvation pressure is defined as $(\partial \Delta G^{\ddagger}/\partial \bar{V})_T$, where $\bar{V}$ is the reactant molar volume. It is identified with the difference in the amount of isothermal work, per unit volume expansion necessary to create a solvation cavity in a particular medium, upon transition-state complex formation. The quantity was evaluated for the hydrolysis of carboxylic esters mediated by different hydrophobic catalysts and was found to be equal to +26 J cm^{-3} for the acid-catalyzed hydrolysis of *n*-alkyl acetates in water solvent; but it becomes negative when macro- or supramolecular acids were used as catalysts: −16 J cm^{-3} for Dowex 50W-X2, −43 J cm^{-3} for poly(styrenesulfonic acid), −64 J cm^{-3} for dodecylsulfuric acid micelles. These results suggest the action of hydrophobic forces in enhancing the catalytic power of the supermolecules, relative to aqueous hydrogen ion. No such effect is seen in aqueous acetone or when more hydrophilic acetates are used as substrates. Kinetic solvation pressure for enzyme-catalyzed ester hydrolysis is five times more negative than for the resin system, indicating the full action of hydrophobic forces in the catalytic process.

The effect of solvent on reaction rates is a fundamental and yet unsolved problem in chemical kinetics, because formal calculation of partition functions for reactants and transition-state (TS) complexes in the liquid state is too difficult.

The traditional approach has been to correlate activation free energies (or log *k* values) with physical properties of the solvent such as dielectric constant, viscosity, and Hildebrand solubility parameters[3] or with a vast array of empirical solvent parameters.[4] The electric field of solute molecules causes changes in the solvent liquid structure in their immediate microenvironment and, therefore, the direct use of bulk solvent properties seems not likely to be adequate.

I propose in this paper an alternative way to obtain a view of solvent-solute interactions, with further applications to macro- and supramolecular catalysts.

Statement of the Model: Solvation Pressures. Let a chemical process occur in a certain solvent at constant temperature and pressure and, further, let the molecules be dissected into a reactive group and an appendage (e.g., an alkyl chain). Figure 1 gives

(1) Resin Catalysis 4. For part 3, see: Reference 28.
(2) Research Fellow of the National Research Council of Costa Rica (CONICIT).
(3) Moore, J. W.; Pearson, R. G. *Kinetics and Mechanism*, 3rd ed., Wiley: New York, 1981; p 244.
(4) Abraham, M. H. *Pure Appl. Chem.* **1985**, *57*, 1055.

0002-7863/88/1510-6224$01.50/0